Available online at www.sciencedirect.com
ScienceDirect
Polymer 49 (2008) 1398–1406
polymer
www.elsevier.com/locate/polymer

Efficient modeling of polysaccharide conformations based on Small-Angle X-ray Scattering experimental data

Iztok Dogsa [a], Janez Štrancar [a], Peter Laggner [b], David Stopar [c,*]

[a] *Jozef Stefan Institute, Laboratory for Biophysics, Jamova 39, 1000 Ljubljana, Slovenia*
[b] *Institute of Biophysics and Nanosystems Research, Austrian Academy of Sciences, Schmiedlstraße 6, A-8042 Graz, Austria*
[c] *University of Ljubljana, Biotechnical faculty, Department of Food Technology, Laboratory of Microbiology, Večna pot 111, 1000 Ljubljana, Slovenia*

Received 23 November 2007; received in revised form 15 January 2008; accepted 15 January 2008
Available online 26 January 2008

Abstract

Small-Angle X-ray Scattering (SAXS) curves of pullulan oligomers and gellan gum were modeled with a new string of beads model. The model enables one to simulate polysaccharide single helices with different pitch values, number of monomers per pitch, and cross-sectional radius, as well as different random coils with excluded volume taken into account. The vast conformational space of possible polysaccharide structures is systematically scanned and, for each selected polysaccharide 3D structure, the SAXS curve is calculated and compared to the SAXS experimental data. All structures with RMSSD ≤ 1 are retained as the solutions. By allowing the distribution of equally good solutions to the given experimental SAXS curve, the new model enables one to get a phase space of possible polymer structures in the aqueous environment. Most importantly it avoids using pre-assumed secondary structure elements to fit the experimental data.

Keywords: SAXS; Structure; Polysaccharides

1. Introduction

Carbohydrates are the most abundant biological molecules. Most carbohydrates found in nature are polysaccharides, polymers of high molecular weight [1]. They are used as food, storage components, or structural elements in plants and animals. Both bacteria and archaea have cell wall composed of polysaccharides, which are essential in cell adhesion [2–5], biofilm formation [5–7], and protect cells from hostile environment [7,8]. Structures of polysaccharides differ from other biopolymers. This is primarily due to the presence of multiple hydroxyl groups, which may form glycoside or hydrogen bonds. For instance, 21 different compounds can be formed by condensation between two D-glucose units [9]. There can be, theoretically, more than 10^{12} different isomers of a hexasaccharide, which is seven orders of magnitude higher than in hexapeptide [10]. In comparison with proteins and nucleic acids, substantial hydrophobic elements, which stabilize structure, are less prevalent [11]. Whereas all natural proteins and nucleic acids are polyions, polysaccharides may or may not be ionic. All of these factors contribute to the enormous conformational space of polysaccharides [11] and present a major challenge for polysaccharide structure determination. There have been important advances made in the study of conformational properties of polysaccharides by NMR spectroscopy, energy calculations [12–17], as well as different light scattering techniques [18]. In particular the Small-Angle X-ray Scattering (SAXS) is a powerful technique revealing structural information on the 1–100 nm scale, which is typically inaccessible by other techniques.

Generally, the proposed structure of the polysaccharide is defined with a set of structural parameters related to SAXS curve by an analytical function $I(q)$. The structural parameters of polysaccharide are extracted by fitting this function to the experimental data. Unfortunately, the assumption about the

* Corresponding author. Tel.: +386 1 423 33 88; fax: +386 1 257 33 90.
E-mail addresses: iztok.dogsa@ijs.si (I. Dogsa), janez.strancar@ijs.si (J. Štrancar), peter.laggner@oeaw.ac.at (P. Laggner), david.stopar@bf.uni-lj.si (D. Stopar).

0032-3861/$ - see front matter © 2008 Elsevier Ltd. All rights reserved.
doi:10.1016/j.polymer.2008.01.043

secondary structure (e.g. helix [19–21]) needs to be made before fitting the experimental data [22–24]. For polysaccharides where local molecular order is expected to be intermediate between the randomly coiled chain and the rigid helix [25], simple models do not give an acceptable result. To remedy this, a more complex modeling of broken rod-like chains was developed [26,27]. In such models individual segments (i.e. coils or helices) are linked together in a random orientation assuming equal averaged lengths [27], which is an obvious simplification. To improve modeling realism, the length of the rod-like chain segment should be shortened ultimately to the size of an individual monomer. The alternative approach for polysaccharide modeling is based on calculating the energetically favorable structures on the atomistic level. In the past 50 years the popular approach for polymer modeling was Rotational Isomeric State (RIS) model [28], which takes into account the interactions among monomers. The RIS model was successfully applied to various polymers including oligosaccharides [15,29]. Although no a priori assumptions about the chain conformation are necessary, the range of possible conformations is dependant on the choice of the type of the force field [14,30]. In addition, the energy calculation makes the simulation relatively complex, computationally demanding, and ignores interactions between residues that are not the nearest neighbors in the primary sequence [25]. Therefore new modeling approaches that are acceptable both in terms of versatility and computation time should be developed.

In the new model described in this article, the monomers are joined in the polymer chain as a string of beads in the 3D space. The polymer structure is resolved by taking into account the geometrical properties of the polymer chain. This is possible since SAXS curve directly depends on the scattering length density distribution in the structure. No a priori assumptions about the chain conformation are necessary. The model has been successfully applied to pullulan oligomers and gellan gum.

2. The model and computational procedures

2.1. Representative chain form factor $\overline{P(q)}$

In the simulation the individual monomers are modeled as spheres joined in the polymer chain as string of beads in the 3D space. The position of the monomer relative to its predecessor in the chain is described by Θ (bond) and Φ (torsion) angles (Fig. 1). The angle pair is assigned to each monomer added to a growing polymer chain. For example, in a helical polymer both Θ and Φ angles are fixed throughout the entire chain. The fixed values of Θ and Φ are denoted as Θ_p and Φ_p. The probability of the random variation of the bond and torsion angles between successive beads is, in the case of a straight single helix, equal to 0 ($p = 0$). On the other hand, in the completely random coil each monomer torsion and bond angles are picked at random with the probability equal to 1 ($p = 1$). The random coil in our simulation, however, is not an ideal chain, since, due to the excluded volume

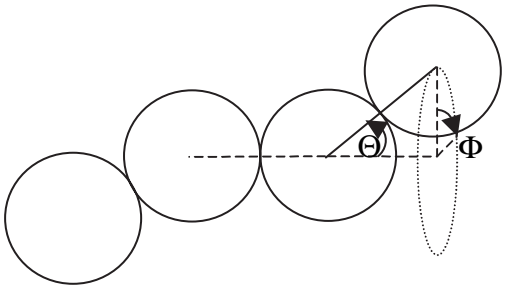

Fig. 1. The schematic representation of bond angle Θ and torsion angle Φ between successive monomers in the modeled polymer chain.

principle, the monomer overlapping is not allowed. This effect cannot be predicted analytically. In general, however, polysaccharide chains tend to adopt intermediate structures that deviate from the perfect helical or entirely random coiled structure [25]. By varying the probability, p, the intermediate structures between a straight helix and a random coil are obtained. For example, if $p = 0.7$ there is a 70% chance that each Θ and Φ angle will be picked at random and 30% chance that Θ and Φ will take some preset value, Θ_p and Φ_p. To vary the stiffness of a polymer chain an additional parameter, Θ_{plim}, is introduced. This parameter sets the upper limit of the bond angle Θ in the simulation. The shape of the polymer is thus fully determined by the choice of Θ_p, Φ_p, Θ_{plim} and p. The p has no meaning in a dimer, since Θ and Φ angles are not defined there. Therefore the fraction of random monomers in polymer is $(N-2)/N \times p$. Furthermore the last monomer in the polymer contributes only half of the impact compared to the rest of the monomers. To correct for this, the effective probability, p^* is introduced as:

$$p^* = \frac{(N-2.5)}{N} p \quad \text{where } N \geq 3 \tag{1}$$

The positions of monomers in the 3D polymer structure, modeled as described above, were converted into a pair-distance histogram $g(r)$. The following computational efficient expression already used by Pantos et al. and van Garderen et al. [31–33] on the basis of Debye formula [34] was used to obtain a single polymer chain form factor $P(q)$:

$$P(q) = F_s^2(q)\left[N + 2\sum_{i=1}^{N_{bins}} g(r_i)\frac{\sin qr_i}{qr_i}\right] \tag{2}$$

where N is the total number of spheres in the system, r_i is the pair-distance between two spheres, $g(r_i)$ is the pair-distance histogram with a bin-width commensurate with the experimental resolution. $F_s(q)$ is the form factor of a sphere with radius R, uniform scattering length density ρ and volume V defined as:

$$F_s(q) = V\rho\left[3\frac{\sin(qR) - qR\cos(qR)}{(qR)^3}\right] \tag{3}$$

The simulation of the single chain with input parameters N, R, Θ_p, Φ_p, Θ_{plim}, p was performed up to 100,000 times and the

calculated single chain structure factors $P(q)$ (Eq. (2)) were averaged to obtain the representative chain form factor $\overline{P(q)}$. The automatic scan through the range of shape parameters (v_p, Φ_p, Θ_{plim}, and p) was performed and for each combination of parameters, a representative chain form factor $\overline{P(q)}$ was obtained, creating a population of representative chain form factor $\overline{P(q)}$. Typically around 60,000 curves with different shape parameters (Θ_p, Φ_p, Θ_{plim} and p) were created. The ranges of parameters and the corresponding step sizes are given in Table 1.

2.2. Interaction terms

Often polymer chains are not uniformly distributed in the solution, i.e. interactions may occur, and additional knowledge about the chain's spatial distribution is necessary. To account for the interaction between neighboring chains one usually combines chain structure factor with interaction terms. Fitting algorithm in our simulation model can select between two different interaction modes: (i) no interaction; (ii) repulsive Gaussian-type interaction.

2.3. No interaction

For non-interaction system the total scattering intensity is given by:

$$I(q) = B\overline{P(q)} \tag{4}$$

where B is the constant proportional to concentration and $\overline{P(q)}$ is the simulated representative chain form factor.

2.4. Repulsive Gaussian-type interaction

The polymer chains can be charged and consequently repel each other. Although more sophisticated approaches on polymer interaction potentials exist [35–37], we employ here the repulsive Gaussian interaction as used by Coviello et al. [17] and Yuguchi et al. [38]:

$$I(q) = \frac{B}{1 + K\exp\left(-\xi^2 q^2\right)}\overline{P(q)} \tag{5}$$

Here, B is the constant proportional to concentration, and Gaussian-type interacting potential is approximately expressed by the correlation length, ξ, and constant K, which is proportional to the polymer concentration and strength of the interaction. Variables B, K and ξ are fitting parameters.

Table 1
Range of shape parameters and step size in the string of beads model

Shape parameter	Range	Step size
Θ_{plim} [rad]	0–2.094	0.25
Θ_p [rad]	0–2.094	0.10
Φ_p [rad]	0–3.14	0.10
p	0–1	0.05

2.5. Experimental data

The experimental SAXS data of pullulan oligomers and gellan gum were kindly provided by Brant [13] and Yuguchi [39], respectively.

2.6. Fitting experimental data

The fitting algorithm fits the experimental data with Eqs. (4) and (5). No a priori assumption of the shape of the chain was given. The fitting algorithm first picks a representative chain form factor $\overline{P(q)}$ and interaction parameters are estimated by bisection method. All representative chain form factors, $\overline{P(q)}$, created during simulation, are probed in this way. The measure for the goodness-of-fit was RMSSD (Root Mean Squared Scaled Deviation):

$$\mathrm{RMSSD} = \sqrt{\sum_{i=1}^{k}\frac{\left(\frac{m_i - d_i}{s_i/\sqrt{n}}\right)^2}{k}} = \sqrt{\frac{n}{k}\sum_{i=1}^{k}\frac{(m_i - d_i)^2}{s_i^2}} \tag{6}$$

where m_i is the theoretical mean of $I(q)$ of each data point, d_i is the mean value of each experimental $I(q)$ data point, s_i is the standard deviation of each experimental $I(q)$ data point, n is the number of data points contributing to each data mean d_i, and k is the number of data points in the experimental $I(q)$ scattering curve. The difference between the experimental $I(q)$ and model $I(q)$, $(m_i - d_i)$, is compared to standard error of the experimental $I(q)$ mean, rather than to standard deviation. The advantages of this measure of goodness-of-fit are thoroughly explained by Schunn and Wallach [40]. The program only retained fits with RMSSD ≤ 1, although one can arbitrarily specify a different less stringent limit in the program. The RMSSD below 1 indicates that model has reached the fidelity of the experimental data and thus the obtained fits are equally good. The number of good solutions therefore depends on the experimental data quality and structural complexity. If structures do not differ enough, e.g. the step size of parameter scan is too small, the fitting algorithm will recognize corresponding form factors as indistinguishable. With a larger experimental q scale, however, one can get a better resolution in solution space.

The simulation program displays solutions of the fitting procedure using shape parameters (Θ_p, Φ_p, Θ_{plim}, p^*) in a 4D cube. The 4D cube is depicted in Fig. 2. Each 3D polymer structure is determined by a combination of the shape parameters. When $p^* = 0$ only straight helices, differing in Θ_p (bond) and Φ_p (torsion) angles, are possible. When p^* increases, more and more monomers have assigned random values of Θ and Φ angles, with the Θ range limited by the value of Θ_{plim}. As a consequence of higher p^*, structures became more similar to random coils. At $p^* = 1$, all the monomers have assigned random values of Θ and Φ angles. Here the structures are governed by the excluded volume principle and Θ_{plim}.

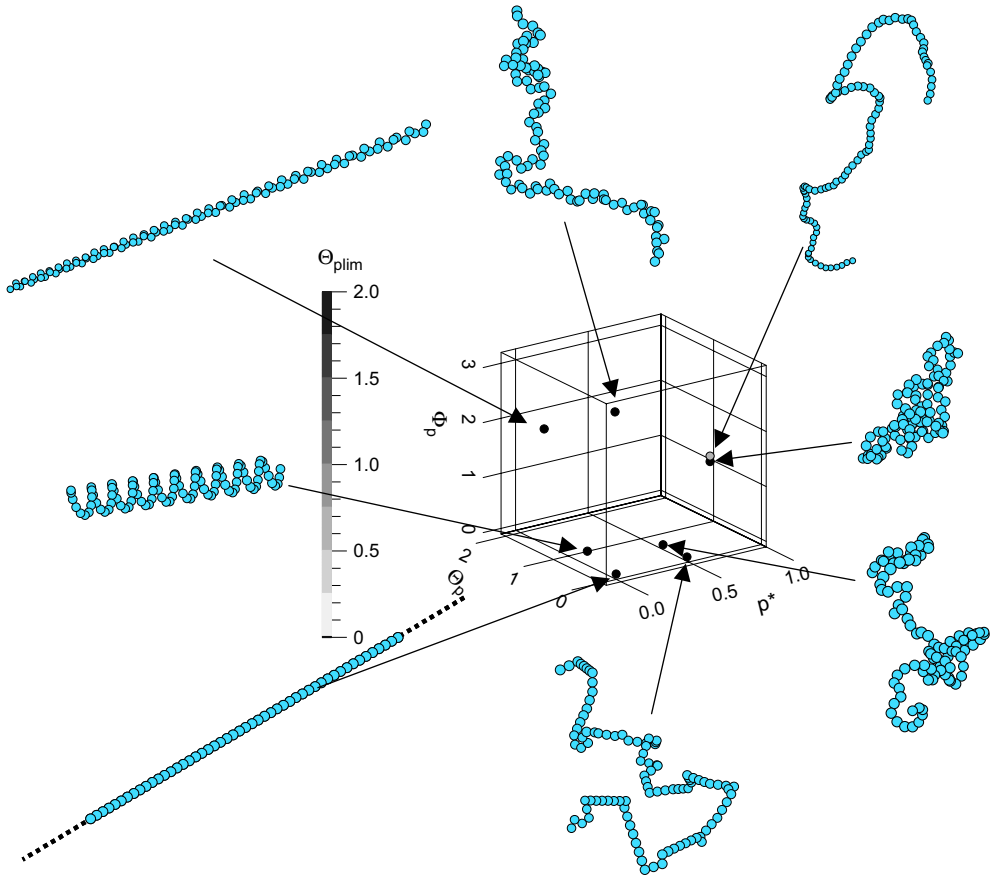

Fig. 2. The 4D cube used to represent the solutions of the fitting procedure to the SAXS experimental data. Each point in the figure represents a possible solution of the polysaccharide structure (a combination of shape parameters p^*, Θ_p, Φ_p and Θ_{plim}); p^* is the effective probability, describing the chance that a monomer will acquire random torsion (Φ) and bond (Θ) angles; Θ_{plim} is the upper limit of the range accessible to bond angle (Θ).

3. Results and discussion

3.1. A comparison of the string of beads model with the atomistic model

In Fig. 3a, an atomistic model of 1,4-α-linked glucose trimer is depicted. To form relatively extended structure the bond and torsion angles between sugar units I–II were chosen to be θ (O_5–C_1–O–C_4') = 92°, φ (C_1–O–C_4'–C_5') = 213°, and for II–III sugar units $\theta = 98°$, and $\varphi = 216°$. The corresponding SAXS curve was calculated using full Debye formula [34] by taking into account all the atoms and their individual atomic form factors, which were calculated using parameterized Gaussian expression as described by Pantos et al. [33]. On the Kratky–Porod graph the dependence of the $I(q)q^2$ for the calculated atomistic structure on the scattering vector q is given. Superimposed on the scattering curve is a fit obtained with the string of beads model. The obtained fit is in an excellent agreement with the atomistic model. The simplified trimer structures that gave the best fit were composed of three connected spheres of the uniform density with a diameter of 5.2 Å. This is consistent with the value of 5.15 Å, which is often taken for the length of anhydroglucose unit [24,41–43]. In Fig. 3b, monomers in the atomistic model of 1,4-α-linked glucose trimer were rotated around their C–O–C bonds. The structure is more condensed with torsion angles for I–II sugar units $\theta = 222°$, $\varphi = 273°$, and for II–III sugar units $\theta = 15°$, $\varphi = 75°$. The corresponding fit obtained from the string of beads model is again in a very good agreement with the atomistic model. The bond angle Θ has increased from 1.00 to 2.07 rad. Similar comparison was also performed on 1,6-α-linked glc trimer, where diameter of the spheres increased from 5.2 to 5.34 Å. In this case a minor deviations in fitted SAXS curves were observed at $q > 4\ nm^{-1}$. From these results it follows that sugar monomers may be reliably represented as spheres when $q < 4\ nm^{-1}$. Compared to atomistic model, however, there is a significant decrease in computation time, if one uses a string of beads model. Even if we neglect scattering from H atoms, the remaining 11 C and 11 O atoms belonging to each glucose residue demand 120 times longer calculating time compared to the string of beads model. Computational time saving with string of beads model is essential, if one wants to simulate larger polymeric molecules.

3.2. Pullulan

Before turning our attention to a large system we apply the new model on a set of pullulan oligomers. Pullulan, an extracellular polysaccharide produced by a fungus *Aureobasidium*

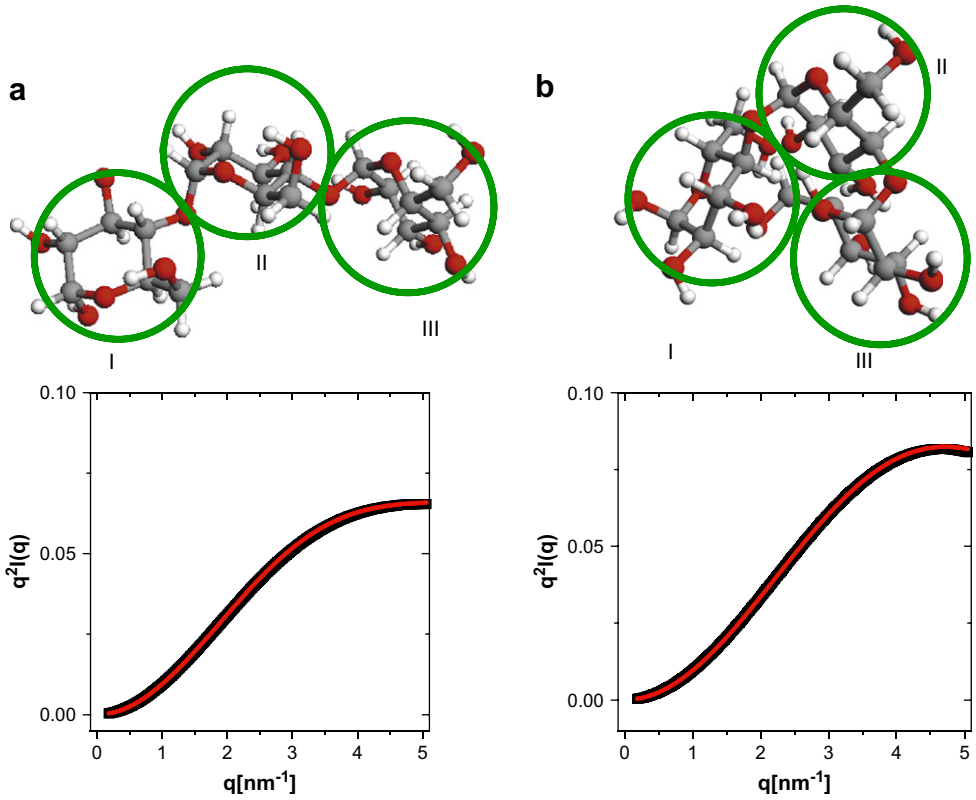

Fig. 3. Comparison between atomistic model and string of beads model: (a) relatively extended conformation of glc trimer is modeled by atomistic model (black curve), superimposed is a red curve obtained by string of beads model; (b) glc trimer structure was rotated around C–O–C glycoside bonds to form a more condensed structure. [For interpretation of the reference to color in this figure legend, the reader is referred to the web version of this article.]

pullulans, is a linear glucan composed of 1,6-α-linked 1,4-α-D-maltotriose units. The SAXS curves of aqueous pullulan trimer (G3), hexamer $(G3)_2$, nonamer $(G3)_3$ and dodecamer $(G3)_4$ are given in Fig. 4. The absence of strong scattering at small q suggests no significant large-scale interactions. The assumption about the absence of the large-scale interactions was already made by several authors considering SAXS curves of pullulan oligomers [13,15,16]. Consistently, there was no need to use the interaction term to fit the experimental scattering curves.

As reported by Liu et al. [15], the samples of individual oligomers, from which SAXS experimental data originate, contained also a small fraction of shorter oligomers. For example, the dodecamer $(G3)_4$ sample contained 64.0% (w/w) dodecamers, 14.9% nonamers, 7.0% hexamers and 14.1% trimers. We took polydispersity into account by first fitting the sample of the homogenous pullulan trimer (G3). The representative chain form factor $\overline{P(q)}$ of the best fit for the trimer sample, weighted by the appropriate fraction, was subsequently used as an additional term in Eq. (4) to fit the hexemer $(G3)_2$ sample. The best representative chain form factor $\overline{P(q)}$ for nonamer and dodecamer was obtained similarly. The solutions for oligomers' shape parameters (Θ_p, Φ_p, Θ_{plim}, p^*) are shown in 4D cubes in Fig. 4. All the points correspond to the equally good fits to the experimental data under stringent conditions (i.e. RMSSD ≤ 1). On the right hand side in Fig. 4 a sample structure corresponding to a central point in the 4D cube of possible solutions is shown. The numerical values of the parameters for the sample structures are given in Table 2. In the case of pullulan trimer, the torsion angles are not defined since the structure has only three monomers. Consequently a large distribution along a torsion angle Φ_p of equally good solutions (RMSSD ≤ 1) is displayed. Pullulan trimer has 1,4 bonds only. As can be observed from the simulation results, the bond angle Θ_p has not exceeded 0.8 rad, suggesting that trimer is relatively extended. An increase in p^* is accompanied by a decrease in Θ_{plim}. Since Θ_{plim} limits the range of possible bond angles this suggest a restricted flexibility of the trimer. From the potential surface energy calculations and molecular dynamics simulations [13,15,16] it follows that 1,4 bonds are relatively rigid and extended. In the case of pullulan hexamer one out of six monomers has 1,6 bond, which is a much more flexible conformation than 1,4 bond conformation [13,15,16]. As expected, Θ_p, Θ_{plim} and p^* are higher than in the case of trimer. Similarly, the flexibility of the nonamer is higher than that of the trimer. The comparison of the flexibility of nonamer and hexamer was not possible, since solutions in 4D cubes overlapped. In the case of dodecamer 3 out 12 monomers have 1,6 bond. The value of p^* has increased compared to the nonamer, indicating higher proportion of the random structure. At the same time, Θ_{plim} and Θ_p remained relatively high. Together this suggests that dodecamer has the most flexible structure of the evaluated oligomers. The modeling by Buliga and Brant [44] indicated

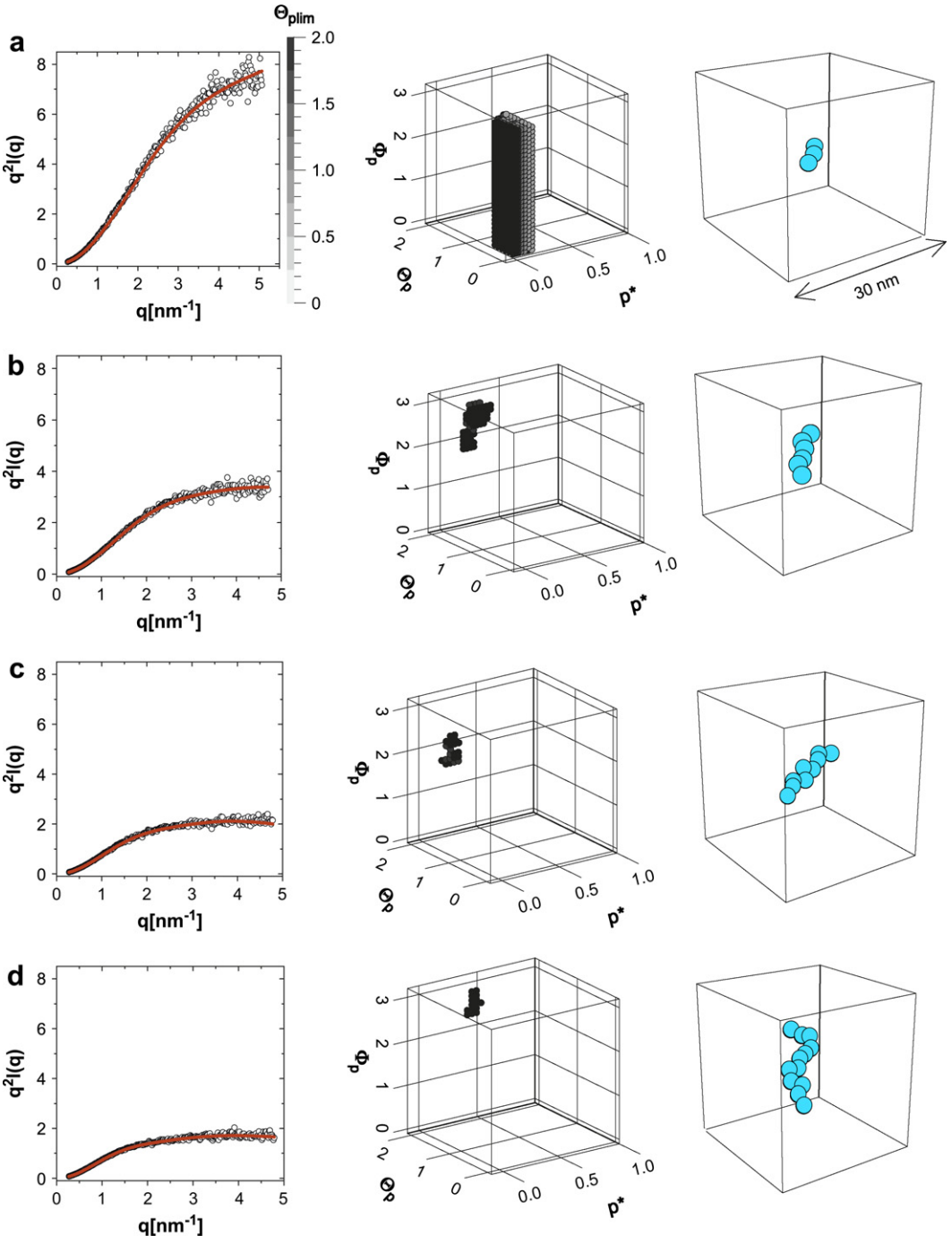

Fig. 4. The Kratky–Porod graphs of pullulan trimer (a), hexamer (b), nonamer (c) and dodecamer (d). Experimental SAXS data (○) string of beads model (●). Each point in the 4D cubes is a solution of the fitting algorithm that gives equally good fit (i.e. RMSSD ≤ 1). The sample structure, corresponding to the central point in 4D solution cube, is given in the right hand side. Values of p^*, Θ_p, Φ_p and Θ_{plim} for the sample structure are given in Table 2. The experimental SAXS data were kindly provided by Brant [13].

that the directional correlations of the successive bonds in the aqueous pullulan polymer chain are lost completely over the range of approximately 15 residues. Similar results were also obtained by ^{13}C NMR study of pullulan polymers [45]. Although a 15-residue pullulan has not been modeled in this study, we have observed that directional correlations of the successive bonds vanished almost completely already in dodecamer. The changes of the experimental curves in Fig. 4 are not only due to changes in the shape parameters, but also because of the increasing number of monomers per oligomer and larger radius of gyration. The radius of gyration was determined from scattering curves of sample structures by evaluating the initial slope of a plot $\ln(\overline{P(q)})$ against q^2 according to Guinier law. The values given in Table 2 are in a good agreement with the R_g obtained by other authors [13,15,16].

Table 2
Values of p^*, Θ_p, Φ_p and Θ_{plim} for the sample structures given in Figs. 4 and 5

Sample structures	T_{plim} [rad]	T_p [rad]	F_p [rad]	p^*	R_g [Å]
Pullulan trimer	1.00	0.40	0.70	0.04	4.7
Pullulan hexamer	1.75	1.60	2.61	0.18	6.7
Pullulan nonamer	1.75	1.70	2.16	0.22	8.5
Pullulan dodecamer	2.00	1.80	2.66	0.44	10.2
Gellan I	1.00	0.70	1.38	0.00	
Gellan II	1.50	0.40	1.73	0.05	
Gellan III	0.75	0.50	1.53	0.15	
Gellan IV	0.75	0.50	2.84	0.40	

3.3. Gellan gum

This is a linear polymer composed of tetrasaccharide repeat units: 1,3-β-D-glucose, 1,4-β-D-glucuronic acid, 1,4-β-D-glucose and 1,4-α-L-rhamnose produced by *Pseudomonas elodea*. The structure and the impact of different experimental physico-chemical conditions on structural properties of gellan gum are well documented [38,39,46–57]. The M_w reported for non-native gellans ranges from 170 kDa up to 360 kDa [46–49]. For the simulation purpose an average reported value of 250 kDa has been selected, which corresponds to 1570 monomer units. The experimental SAXS curve for the gellan gum (1% w/v) at room temperature without added salt is given in Fig. 5. There was no model solution obtained without taking an electrostatic interaction term into account. The problem was that the model without the interaction term could not account for the broad peak around $q = 0.5\ \mathrm{nm}^{-1}$. It was shown before that polyelectrolytes such as, for example, polystyrene-sulfonic acid [58], poly(*p*-phenylene) [59] or polysaccharide sclerox [17] exhibit broad peak at large q, which was attributed to the electrostatic interaction. Gellan is a polyelectrolyte and by taking the electrostatic Gaussian repulsive potential into account (Eq. (5)) we were able to fit the SAXS curve. The electrostatic interaction correlation length, ξ, obtained from the fit was 29 ± 1 Å, which is similar to the value of 31.6 Å, obtained by Yuguchi et al. [38]. As a result of their modeling, Yuguchi et al. [38] obtained straight single helix structure of gellan gum. Based on a limited number of secondary structures used in their modeling, they could discriminate between the straight single helix and perfect random coil. Although their fit indicates the prevalence of straight single helix structure other less ordered secondary structures could not be ruled out from the experimental data. As can be seen from Fig. 5, straight single helix is one of the possible solutions (i.e. at $p^* = 0$). However, several other equally good solutions (RMSSD ≤ 1) are obtained as well. The effective probability p^* in the range from 0 to 0.45 suggests that in addition to the straight helix other gellan gum conformations with higher

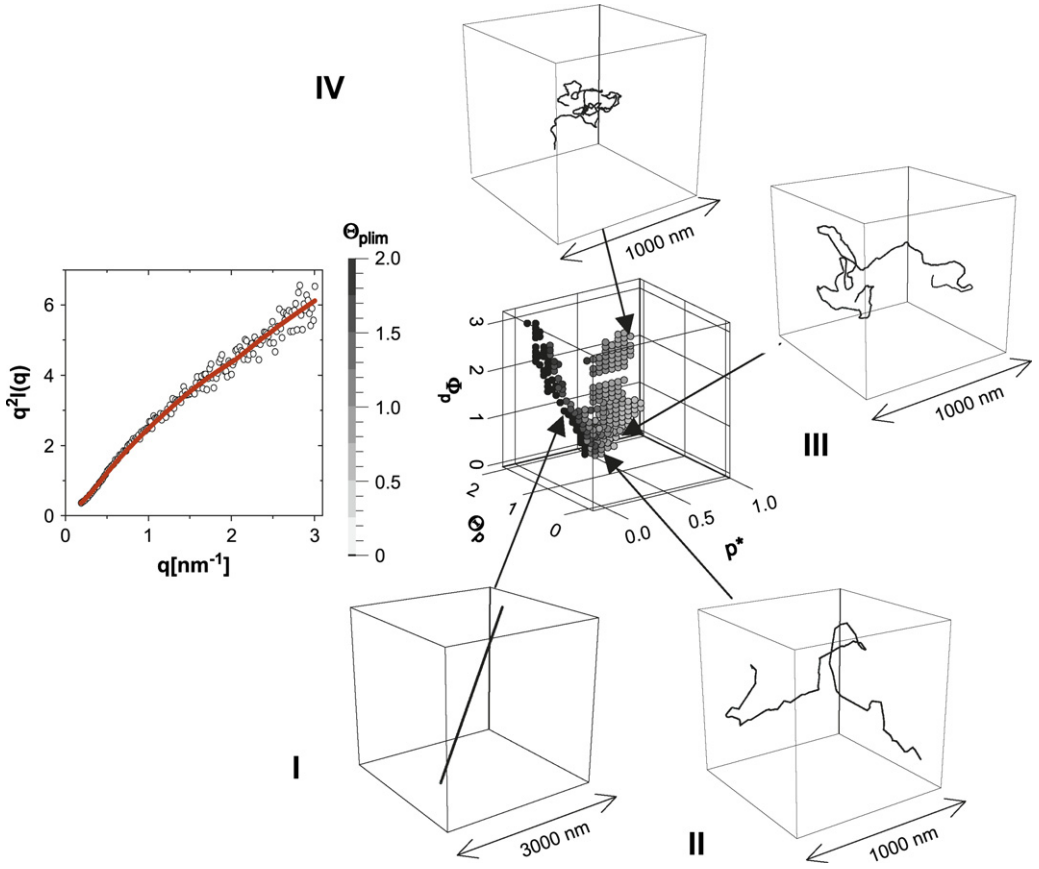

Fig. 5. The Kratky–Porod graphs of gellan gum. Experimental SAXS data (○) string of beads model (●). Each point in the 4D cubes is a solution of the fitting algorithm that gives equally good fit (RMSSD ≤ 1). The sample structures are given in the right hand side. The values of p^*, Θ_p, Φ_p and Θ_{plim} for the sample structures are given in Table 2. The experimental SAXS data were kindly provided by Yuguchi [39].

proportion of the random structure are possible. Careful observation of 4D cube of solutions reveals that by increasing p^*, Θ_{plim} decreases which makes gellan gum structures stiff and rod-like. This is expected since the line shape of the SAXS curves for gellan gum is typical for rod-like particles [60]. As shown in Fig. 5, most of the sample structures of gellan gum look like a curved thread composed of rod-like segments. It is important, however, to be aware of the large spatial scale on which gellan gum appears to be curved. On the small scale, gellan gum is still predominantly helical. The rheological studies done under similar experimental conditions (no added salt, 1% w/v gellan gum concentration) imply that the transition temperature from helix to single coil is between 20 and 30 °C [50,51]. Therefore it is reasonable to expect that at room temperature gellan gum will be mainly a single helix with some inherent randomness. Such solutions have non-zero effective probability p^* in Fig. 5 and make the majority of solutions.

4. Concluding remarks

Structure determination of polysaccharides in a solution is a difficult subject. In this work we have developed a new string of beads molecular model for structural determination of polysaccharides in solutions based on SAXS curves. The modeling approach used is satisfactory both in terms of versatility and computation time. The new model has been successfully applied to different unrelated linear saccharides such as pullulan oligomers and gellan gum. The model has not been tested for double and triple helices or non-linear polysaccharides. Using the new model one is able to extract structural parameters from SAXS curves such as bond and torsion angles and degree of randomness in the structure, which is not easily obtained by other methods. By semi-coarse-grained description of the polymer chain with beads representing the whole monomers, however, the precise information about the microscopic states is lost. When precise microscopic information is required, the atomistic modeling using energy constraints, as for example in RIS, is a preferred method of choice. Nevertheless, as can be inferred from Fig. 3, the correspondence between the atomistic model and string of beads model is very good. Important advantage of our model is its ability to obtain a distribution of equally good solutions of the polymer structure. Most importantly, the new model avoids using pre-assumed secondary structure elements to fit the experimental data and offers a valuable new tool in polysaccharide research.

References

[1] Lehninger AL, Nelson DL, Cox MM. Principles of biochemistry. New York: Worth Publishers Inc.; 1997.
[2] Tsuneda S, Aikawa H, Hayashi H, Yuasa A, Hirata A. FEMS Microbiol Lett 2003;223:287.
[3] Frank BP, Belfort G. J Membr Sci 2003;212:205.
[4] Joyce JG, Abeygunawardana C, Xu Q, Cook JC, Hepler R, Przysiecki CT, et al. Carbohydr Res 2003;338:903.
[5] Sutherland IW. Adv Microb Physiol 1972;8:143.
[6] Cescutti P, Toffanin R, Pollesello P, Sutherland IW. Carbohydr Res 1999;315:159.
[7] Decho AW. Cont Shelf Res 2000;20:1257.
[8] Looijesteijn PJ, Trapet L, de Vries E, Abbe T, Hugenholtz J. Int J Food Microbiol 2001;64:71.
[9] Perez S, Kouwijzer M, Mazeau K, Engelsen SB. J Mol Graphics 1996;14:307.
[10] Laine RA. Glycobiology 1994;4:759.
[11] Brant AD. Pure Appl Chem 1997;69:1885.
[12] Kitamura S, Minami T, Nakamura Y, Isuda H, Kobayashi H, Mimura M, et al. THEOCHEM 1997;395–396:425.
[13] Liu JH-Y, Brant DA, Kitamura S, Kajiwara K, Mimura M. Macromolecules 1999;32:8611.
[14] Shimada J, Kaneko H, Takada T, Kitamura S, Kajiwara K. J Phys Chem B 2000;104:2136.
[15] Liu JHY, Brameld KA, Brant DA, Goddard WA. Polymer 2002;43:509.
[16] Jaud S, Tobias DJ, Brant DA. Biomacromolecules 2005;6:1239.
[17] Coviello T, Maeda H, Yuguchi Y, Urakawa H, Kajiwara K, Dentini M, et al. Macromolecules 1998;31:1602.
[18] Brant AD. Curr Opin Struct Biol 1999;9:556.
[19] Rundle RE, French DJ. J Am Chem Soc 1943;65:1707.
[20] Arnott S, Scott WE, Rees DA, McNab CGA. J Mol Biol 1974;90:253.
[21] Arnott S, Fulmer A, Scott WE, Dea ICM, Moorhouse R, Rees DA. J Mol Biol 1974;90:269.
[22] Draget KI, Stokke BT, Yuguchi Y, Urakawa H, Kajiwara K. Biomacromolecules 2003;4:1661.
[23] Dogsa I, Kriechbaum M, Stopar D, Laggner P. Biophys J 2005;89:2711.
[24] Hirata Y, Sano Y, Aoki M, Shohji H, Katoh S, Abe J, et al. Carbohydr Polym 2003;53:331.
[25] Perez S, Mazeau K, Herve du Penhoat C. Plant Physiol Biochem 2000;38:37.
[26] Muroga Y. Macromolecules 1988;21:2751.
[27] Muroga Y. Macromolecules 1992;25:3385.
[28] Helfer C, Mattice W. The rotational isomeric state model. In: Mark JE, editor. Physical properties of polymers handbook. New York: Springer; 2007. p. 43–57.
[29] Brant DA, Goebel KD. Macromolecules 1975;8:522.
[30] Perez S, Imberty A, Engelsen SB, Gruza J, Mazeau K, Jimenez-Barbero J, et al. Carbohydr Res 1998;314:141.
[31] Garderen HF, Pantos E, Dokter WH, Beelen TPM, Santen RA. Modell Simul Mater Sci Eng 1994;2:295.
[32] Pantos E, Bordas J. Pure Appl Chem 1994;66:77.
[33] Pantos E, van Garderen HF, Hilbers PAJ, Beelen TPM, van Santen RA. J Mol Struct 1996;383:303.
[34] Debye P. Ann Phys 1915;46:809.
[35] Bolhuis PG, Louis AA, Hansen JP, Meijer EJ. J Chem Phys 2000; 114:4296.
[36] Likos CN, Rosenfeldt S, Dingenouts N, Ballauff M, Lindner P, Werner N, et al. J Chem Phys 2002;117:1869.
[37] Massiera G, Ramos L, Pitard E, Ligoure C. J Phys Condens Matter 2003;15:225.
[38] Yuguchi Y, Mimura M, Urakawa H, Kitamura S, Ohno S, Kajiwara K. Carbohydr Polym 1996;30:83.
[39] Yuguchi Y, Urakawa H, Kajiwara K. Food Hydrocolloids 2002;16:191.
[40] Schunn CD, Wallach D. Evaluating goodness-of-fit in comparisons of models to data; 2001. Online manuscript, http://lrdcpittedu/schunn/gof/indexhtml.
[41] Laivins GV, Gray DG. Macromolecules 1985;18:1746.
[42] Hoogendam CW, de Keizer A, Cohen Stuart MA, Bijsterbosch BH, Smit JAM, van Dijk JAPP, et al. Macromolecules 1998;31:6297.
[43] Arguelles-Monal W, Cabrera G, Peniche C, Rinaudo M. Polymer 2000; 41:2373.
[44] Buliga GS, Brant DA. Int J Biol Macromol 1987;9:77.
[45] Banesi AJ, Brant DA. Macromolecules 1985;18:1109.
[46] Milas M, Shi X, Rinaudo M. Biopolymers 1990;30:451.
[47] Okamoto T, Kubota K, Kuwahara N. Food Hydrocolloids 1993;7:363.
[48] Miyamoto K, Tsuji K, Nakamura T, Tokita M, Komai M. Carbohydr Polym 1996;30:161.

[49] Dreveton E, Monot F, Lecourtier J, Ballerini D, Choplin L. J Ferment Bioeng 1996;82:272.
[50] Miyoshi E, Takaya T, Nishinari K. Thermochim Acta 1995;267:269.
[51] Miyoshi E, Takaya T, Nishinari K. Carbohydr Polym 1996;30:109.
[52] Yuguchi Y, Urukawa H, Kitamura S, Wataoka I, Kajiwara K. Prog Colloid Polym Sci 1999;114:41.
[53] Dentini M, Coviello T, Burchard W, Crescenzi V. Macromolecules 1988;21:3312.
[54] Takahashi R, Akutu M, Kubota K, Nakamur K. Prog Colloid Polym Sci 1999;114:1.
[55] Milas M, Rinaudo M. Carbohydr Polym 1996;30:177.
[56] Ogawa E, Matsuzawa H, Iwahashi M. Food Hydrocolloids 2002;16:1.
[57] Takahashi R, Tokunou H, Kubota K, Ogawa E, Oida T, Kawase T, et al. Biomacromolecules 2004;5:516.
[58] Tomšič M, Bešter Rogač M, Jamnik A. Acta Chim Slov 2001; 48:333.
[59] Guilleaume B, Blaul J, Ballauff M, Wittemann M, Rehahn M, Goerigk G. Eur Phys J E 2002;8:299.
[60] Roe RJ. Methods of X-ray and neutron scattering in polymer science. New York: Oxford University Press; 2000.